Fluorescence imaging to quantify the fluorescent microspheres in cardiac tissue

Gussakovsky, Eugene; Kuzio, Bozena; Yang, Yanmin; Kupriyanov, Valery

National Research Council Canada   Conseil national de recherches Canada

Canada

Fluorescence imaging to quantify the fluorescent microspheres in cardiac tissue

Eugene Gussakovsky[*,1], *Bozena Kuzio*[1], *Yanmin Yang*[2], and *Valery Kupriyanov*[1,2]

[1] National Research Council Institute for Biodiagnostics, Winnipeg, Manitoba R3B 1Y6 Canada
[2] Faculty of Medicine, University of Manitoba, Winnipeg, Manitoba R3E 3P5 Canada

To quantify the fluorescent microsphere (FM) content in cardiac tissue, which is an indicative of blood flow, fluorescence imaging of both sides of the pig heart slice was employed. Despite the light scattering inside the tissue and contributions from multiple tissue layers to the total emission, it is shown that the fluorescence intensity at any pixel is proportional to the FM content and the fluorescence image may be transformed to the image of the FM concentration. A convenient standard for the emission-FM concentration transformation is proposed. The approach has several advantages in comparison with the traditional "digestion & extraction" method such as: non-destructiveness, high spatial resolution, high throughput, repeatability and simplicity of operation.
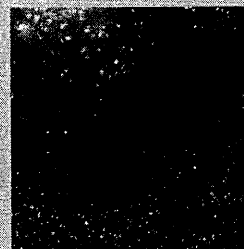
A pig heart slice fluorescence image at resolution of 37.4 μm per pixel.

1. Introduction

Fluorescent microspheres (FM) have been found to serve as an effective tool for the determination of blood flow in various tissues considered to be a gold standard [1–6]. Because the blood flow is a proportional to the microspheres concentration in the tissue, the quantitative microsphere determination in biological tissue is critical.

The standard procedure, a "destruction & extraction" method, consists of the tissue samples preparation, their digestion, FM isolation, fluorophore extraction and fluorescence analysis [1–3]. The procedure has been developed in detail including its automation [7, 8]. Despite high efficiency, a few disadvantages of the fluorescent microsphere technique still exist such as a long time required for tissue processing (hours, days), low spatial resolution and sample destruction. Although automation may reduce the time required, it is still much higher than for radioactive microspheres (RM).

RM lack these disadvantages but create other problems related to the effect of radiation on workers and the environment and the high cost of storage and disposal of waste [4]. Comparison of the RM and FM techniques gives an excellent correlation [4, 9], which forms a basis for the substitution of RM by FM.

Fluorescence imaging of cardiac tissue samples is analyzed in the present paper. It combines advantages of both RM and FM and avoids their disadvantages. The FM-based ultraviolet-excited fluorescence imaging was shown to be an effective tool to qualitatively visualize an ischemic myocardium [10]. Autoradiographic image analysis of RM-labeled myocardial slices is time consuming (hours) and not sufficiently accurate in microsphere content determination [11]. Radiographic imaging with a radionuclide-labeled desmethylimipramine as a deposit tracer was proposed for analysis of myocardial flow heterogeneity with a spatial resolution of $400 \times 400 \,\mu\text{m}$ [12]. The content of the tracer in tissue was not determined.

In an attempt to overcome the limitations of the "destruction & extraction" method, fluorescence imaging of fluorescent microspheres in biomedical samples was employed for qualitative and quantitative characterization of microsphere deposition and blood flow [5, 6, 13]. In particular, fluorescence images of frozen thin $(30 \,\mu\text{m})$ rabbit heart slices were shown to quantify fluorescent microspheres deposited in the cardiac tissue [5].

An advantage of fluorescence imaging of macroscopic samples is the non-invasive analysis of tissue samples as a whole without additional physical or chemical destruction. An optical image is a 2D map of some optical parameter value across the tissue surface. The known inverse problem may be formulated as a determination of fluorescent inclusions in the tissue depth from the 2D intensity distribution [14]. The solution of such problems has been shown to lead to a 3D reconstruction of the spatial distribution of fluorescent sources from initial 2D data [14–16]. This shows that 2D fluorescence images may contain information on 3D concentration images of FM in tissue.

Specific equations have been developed to calculate the total emission of FM, FluoSpheres®, using fluorescent images of cardiac tissue [17]. The equations take into account penetration of the excitation light into the tissue and collection of FM fluorescence emitted from inside the tissue. For slices cut perpendicularly to the long axis of the heart, it was shown that if the distribution of FM content gradually changes across the muscle tissue then the mean FM concentration C_{FM} is proportional to the total fluorescence measured from both sides of the slice [17]:

$$C_{FM} = \kappa \, \frac{F_a + F_b}{2} \qquad (1)$$

where F_a and F_b are fluorescence intensities emitted from the apex and base sides (for definition see Section 2.2) of the slice, respectively,

$$\kappa = \frac{2\mu_s'}{\varepsilon \varphi E_0} \qquad (1a)$$

and $\mu_s' = \mu_s(1 - g)$ is a reduced scattering coefficient depending on an anisotropy parameter g which is about 0.96 for myocardium [18], ε and φ are the extinction coefficient and fluorescence quantum yield of FM, respectively, E_0 is the intensity of the fluorescence excitation light, and μ_s is a scattering coefficient of $16-19 \,\text{mm}^{-1}$ for myocardium at 633 nm [19]. In general, Eq. (1a) should contain a total attenuation coefficient $\mu_t = \mu_a + \mu_s'$. Obviously, μ_s' ranges in $6.4-7.6 \,\text{cm}^{-1}$. A blood-free cardiac tissue contains about 0.3 mM of myoglobin [20], which absorbes light with extinction coefficient about $1 \,\text{mM}^{-1} \,\text{cm}^{-1}$ at $634-636 \,\text{nm}$ [21]. This yields the total absorption of $\mu_a \sim 0.3 \,\text{cm}^{-1}$. Because $\mu_a \cong 0.04\mu_s'$, $\mu_t \cong \mu_s'$ represents the total light attenuation inside a tissue.

In the present work, we show that the fluorescence intensity at each pixel of the 2D fluorescence image is proportional to the FM concentration in the underlying cardiac tissue. This allows mapping the cardiac tissue in units of the microsphere content rapidly, with high spatial resolution, non-destructively, repeatedly and in any region of interest (ROI).

2. Materials and methods

2.1. Fluorescent microspheres

In the present study, FluoSpheres® polystyrene scarlet fluorescent (645/680) microspheres of $15.4 \pm 0.2 \,\mu\text{m}$ diameter (Invitrogen – Molecular probes, Eugene, OR) were used as recommended for blood flow determination [2].

2.2. Heart slices preparation

Pigs of about 26 kg weight received humane care in compliance with the Guidelines of the Canadian Council on Animal Care (Ottawa, 1993). Following acclimatization and fasting, preanesthesia was induced with midazolam, ketamine, and atropine. After endotracheal intubation, the pig was ventilated mechanically with 60/40% oxygen/air. Anesthesia was maintained with isoflurane. See Ref. [22] for detail.

Five ml of sonicated FM suspension $(1 \times 10^6$ beads per ml) were injected through the apex into the left ventricle while the aorta was clamped for a few seconds directing all ejected blood and FM to the coronary circulation. The heart was arrested with cardioplegic solution, which removed blood from vasculature, isolated and cut into slices of 3–6 mm thickness across the heart long axis (from the apex to the base). The slices were stored in a standard buffered formalin solution (3.5% formaldehyde, 33 mM

NaH$_2$PO$_4$, 46 mM Na$_2$HPO$_4$) for up to 1–2 months before the fluorescence images were captured. The slices sides facing the apex or the base are referred apex (A) or base (B) sides, respectively. Fifteen slices of four pigs were cut into 92 slabs, which were used for the FM quantitative analysis as described below.

2.3. Fluorescent microspheres isolation and quantitative dye analysis

Isolation of FM was performed as described elsewhere [2, 4] with minor variations. About 0.5–1 g heart slice tissue slabs were cut into 0.05–0.2 g pieces and digested in Pyrex tubes in 3–3.5 ml of 2 M KOH in 70% ethanol containing 0.5% Tween 80 mixture at 60 °C for 3–4 hours. After centrifugation (20 min; 2000 g), the supernatant was collected and 5 ml of 0.25% Tween 80 were added to about 0.5 ml of the pellet suspension. The suspension was centrifuged (20 min; 2000 g), the supernatant was collected and 5 ml of deionized water were added to the pellet. After centrifugation (20 min; 2000 g) the supernatant was collected and 2 ml of xylene were added to about 0.5 ml of suspension. After thorough vortexing, centrifugation (20 min; 2000 g) allowed separation of the two phases and collection of 1 ml of the FM xylene solution.

Fluorescence at 686–688 nm was measured to determine the concentration of the FM dye in xylene. Solutions in a standard 10 × 10 × 45 mm cuvette were excited at 600 nm and the fluorescence intensity was measured employing a Spex FluoroMax spectrofluorometer (Edison, NJ, USA). To calibrate the fluorescence data in FM concentration units, pre-defined volumes of the FM suspension were dissolved in xylene providing standards of various concentrations. The dependence of pre-defined FM concentration versus fluorescence intensity (Figure 1) was linear with a slope of 1.39 beads/ml per fluorescence arbitrary unit (au), a y-intercept close to zero (−70.5 beads/ml), and a correlation coefficient of 0.995. Such plots were used to calculate the FM concentration in xylene after their isolation from the slabs of the heart (see below).

2.4. Phantom preparation

The phantom was constructed using cotton wool (CW) [23, 24]. Each of four 2.2 ml wells (diameter of 16 mm, depth of 11 mm) in high-density polyethylene (HDPE) plates was filled by 0.3 g cotton wool. Different number of FluoSpheres® was dissolved in xylene resulting in the dye concentrations corresponding to 0.5, 1.0, 2.0 and 3.0 kbeads/ml. CW was wet with 1.2 ml of solution and left for air drying overnight in the light-protected place. Fluorescence imaging was performed from the CW surface facing the CCD camera.

2.5. Fluorescent microspheres on Millipore filter

The stock suspension of FluoSpheres® (see above) was vortexed and diluted with deionized water to a bead concentration of 8 × 10^3 beads/ml. After sonication for 1 min, the resulting suspension was immediately filtered through the 5 μm Millipore filter with an effective diameter of 3.9 mm. Filtration under vacuum led to full removal of the aqueous solvent while FM of 15.4 μm were retained on the filter.

2.6. Fluorescence imaging

Figure 2 shows schematics of the fluorescence image measurements in a chamber (black box, BB). Fluorescence was excited by the light of six 635 nm laser diodes of 5 mW each (Thorlabs, Newton, NJ) emitted a non-collimated elliptical light beam with divergence of about ±5° for the short axis and ±15° for the long axis. The diodes were placed at 17.7 cm from the sample surface. Three diode light beams were incident on the slab or slice surface at the angle $\Theta = 25°$
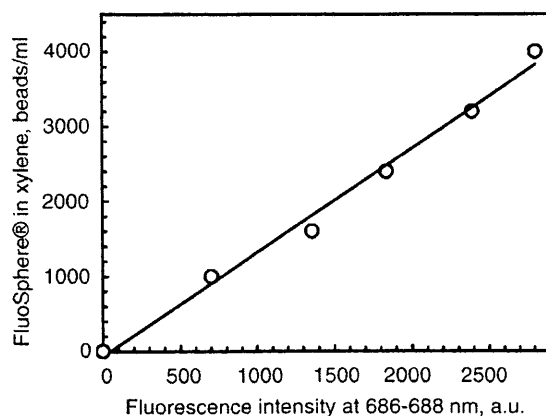

Figure 1 A plot of the FluoSpheres® (FM) concentration in xylene versus the FM dye fluorescence at 686–688 nm. Excitation, 600 nm. Cuvette was equipped with a stopper to prevent the xylene evaporation. Linear regression analysis: slope = 1.39, y-intercept = −70.5, correlation coefficient = 0.995.
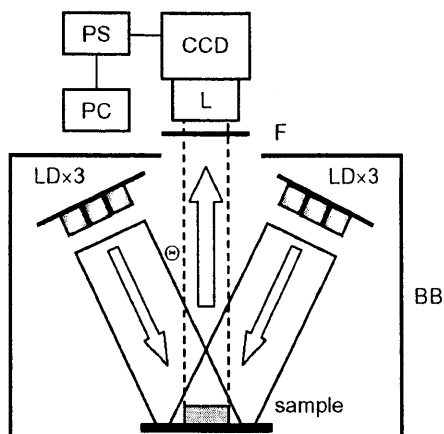
Figure 2 Schematic of fluorescence imaging measurements. BB, black box (chamber); CCD, charge-coupled device camera; F, cutoff glass filter; L, lens; LD, laser diode; PC, computer; PS, power supply and CCD signal amplifier; $\Theta = 25°$, angle of the excitation light beam incidence. LD light is incident on the sample. Emission (dashed lines) is collected on the CCD elements by the lens *via* the cutoff filter. PS amplifies the CCD signal and transfers it to PC resulting in the image capture.

from the normal to the imaging plane. Another three diodes provided illumination at $\Theta = -25°$. Because of the divergence, the individual laser beams overlapped at the sample surface. We considered the total excitation illumination, on average, perpendicular to the sample surface because of equal illumination from the +25° and −25° sides and the non-collimated laser diode beams.

A minimal heterogeneity of such illumination over the surface was corrected for. A Whatmann 3 Qualitative filter paper was soaked with an IR676 infrared dye dissolved in dimethyl sulfoxide. The solvent evaporated leading to homogenious distribution of the dye across the paper. All sample fluorescence images were divided by the image of this dye-containing paper providing the correction for the illumination inhomogeneity.

Fluorescence imaging was performed with two setups. A setup used for slabs fluorescence imaging, consisted of an infrared-sensitive charge-coupled device (CCD) array camera (RS Roper Scientific NTE/CCD-512-EBTF.GR-1, Tuscon, Az) consisted of a 512 × 512 back-illuminated CCD element and 14/16-bit ST-138 analog to digital converter run in 14-bit mode (Princeton Instruments, Trenton, NJ). A 2 × 2 binning reduced the image size to 256 × 256 pixels. It was fitted with a Nikon Micro AF60 lens at f/8 and a LOMO (Russia) KC-18 glass filter, which cuts off the excitation light. See Ref. [17] for more details.

A second setup used for slice fluorescence imaging, consisted of a PixeLINK CCD USB 2.0 PL-B953 monochrome camera of 1024 × 768 pixel resolution allowing a 2 × 2 binning reduced the image size to 512 × 384 pixels. The camera was fitted with a Sigma 24 mm F1.8 EX DG aspherical lens and a Schott RG695 glass filter.

Both KC-18 and RG695 glasses cut off the excitation light (transmittance of 0.2% at 635 nm) and transmits more than half of the FM fluorescence [17].

The images were processed using a Matlab (The MathWorks, Natick, MA) program developed specifically for the current task.

Before imaging, the slices or slabs were washed in deionized water and blotted with paper tissue.

2.7. Statistics

Linear correlations were performed using a least square analysis for linear function [25]. This resulted in the best slope and y-intercept values as well as a linear correlation coefficient. The rest of the data were presented as a mean ± standard deviation.

3. Results

3.1. Phantom measurements

These measurements were performed to verify a reliability of Eq. (1) in artificial well-defined one-side-illuminated $(F_a = F_b)$ samples, which yet mimic cardiac tissue.

There are many phantoms, which have been used to mimic biological tissues, providing diffuse reflectance and suitability for fluorescence measurements [26–28]. Various materials have been used as references for diffuse reflectance spectra determination [29–40]. However, the most suitable for muscle or myocardial tissues is a phantom based on cotton wool [23]. It was used in the present work as closely mimics the fibrous structure of muscles consisting of long muscle and collagen fibers, a capillary network containing an aqueous solution of proteins and suspended blood cells with 80–85% water content in free and bound form, with dye attached to the fibers. It tolerates almost any amount of loaded water allowing adjustment in wide range from zero to 99%. It is a good water sorbent (15–25%) that can also retain free water outside the fibers. The phantom may be prepared in various densities including the density of 1.06 g/cm^3 typical for mammalian muscle [41]. In the present study, we used it as a basic scattering template and FM dye adsorbed on the CW fibers.
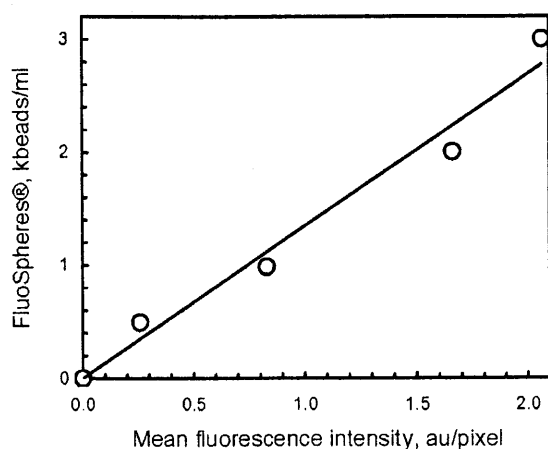
Figure 3 A plot of FluoSpheres® dye content in the FM equivalent in cotton wool versus its mean fluorescence intensity of fluorescence images. Linear regression analysis: slope $= 1.34$, y-intercept $= -0.0017$, correlation coefficient $= 0.976$. For the phantom preparation and fluorescence images measurement detail see Materials and Methods.

Four CW+FM-contained wells were prepared as described in Materials and Methods. A fluorescence image was captured and the fluorescence intensity across each well surface was averaged. Then the related FM-equivalent dye concentration was plotted versus such averaged fluorescence intensity (Figure 3) resulting in a linear correlation with a high correlation coefficient of 0.976, the slope of 1.34 kbeads/ml per a.u./pixel and y-intercept close to zero (-0.0017 kbeads/ml).

This result, that FM fluorescence intensity in the 2D image is proportional to the FM content, supports a reliability of Eq. (1), when $F_a = F_b$, with $\kappa = 1.34$ and uniform distribution of FM in the sample. Such phantom is suitable as a reference at the fluorescence imaging once the κ-value is used to calculate the image of the FM concentration with Eq. (1). It was employed in the current study (see below).

3.2. Fluorescent microspheres in tissue samples

The distribution of FM in the heart is not uniform due to variability in the capillary density [42, 43]. As a first approximation, we considered a gradual change of the FM concentration between apex and base sides of the slice, and compared the FM concentration determined by means of standard biochemical method with both side mean fluorescence $(F_a + F_b)/2$ according to Eq. (1).

The images (Figure 4) and related F_a and F_b were obtained for each of 15 slices of four pig hearts,
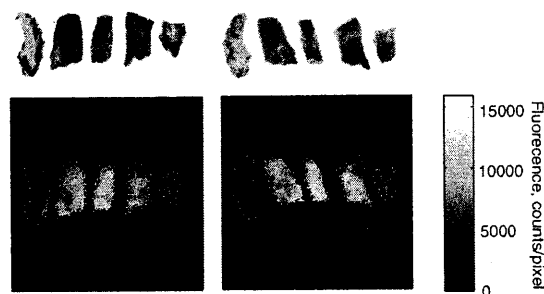

Figure 4 (online color at: www.biophotonics-journal.org) Fluorescence images of two sides of the representative heart slabs. Photographs of the samples are above the images. Excitation, 635 nm. Dotted lines contour the areas, in which the intensities at each pixel were averaged and the plotted versus the FM concentration (Figure 5). See Materials and Methods for detail of the images capture.

which were cut into 92 slabs overall. Afterwards the FM were dissolved in xylene and their content in beads/ml was determined using the calibration coefficient as described in Materials and Methods.

A linear function well fitted the dependence of both side mean fluorescence $(F_a + F_b)/2$ on FM concentrations. Figure 5 shows the data for a represen-
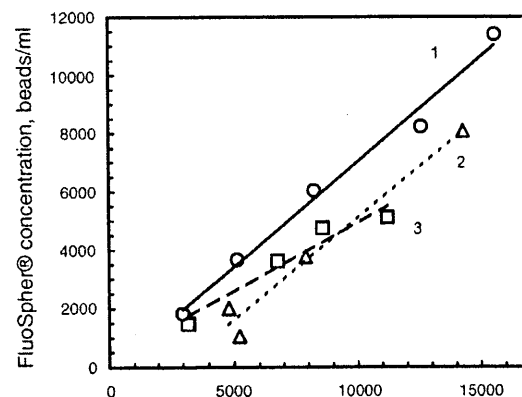
Figure 5 Representative plots of the FM concentration in the tissue samples versus mean emission from these slabs. The mean emission was determined as an average over the contoured slab image (see Figure 4) for two sides of the slab, $(F_a + F_b)/2$. The FM concentration was found by digestion of the piece, extraction of FM, dissolving them in xylene, and fluorescent determination of the dye in solution as described in Materials and Methods. Circles (line 1), triangles (line 2) and rectangles (line 3) refer to three different slices of the same pig heart from which the samples were taken. Linear regression analysis: slope $= 0.722$ (1), 0.702 (2), 0.471 (3); y-intercept $= -195$ (1), -1911 (2), 228 (3); correlation coefficient $= 0.994$ (1), 0.986 (2), 0.968 (3).

Table 1 Parameters of linear correlation between fluorescent microsphere concentration and mean fluorecence intensity.

Pig heart	n	m	slope κ kbeads/ml per count/pixel	y-intercept kbeads/ml	R
A	3	21	1.00 ± 0.24	-6.09 ± 6.76	0.966 ± 0.006
B	4	26	0.39 ± 0.17	-2.58 ± 2.98	0.935 ± 0.028
C	5	25	0.50 ± 0.17	-0.17 ± 0.69	0.960 ± 0.050
D	3	20	0.81 ± 0.24	-0.41 ± 0.44	0.949 ± 0.045
Mean			0.63 ± 0.30	-2.04 ± 3.74	0.952 ± 0.036
Total	15	92			

Notes. For each slice, the FM concentration related to a piece, was plotted versus $I_m = (I_a + I_b)/2$ in counts/pixel as Figure 5 shows. A linear regression resulted in slope κ, y-intercept and correlation coefficient R. The data in the table are mean values and standard deviations over all slices for each heart. n, number of slices; m, number of pieces. Number of pieces varied for different slices. "Mean" slope, y-intercept and correlation coefficient were determined over all slices for all hearts.

tative pig heart. In this particular case, the mean correlation coefficient over all slabs was 0.982 ± 0.011, and the average slope was $\kappa = 0.63 \pm 0.11$ beads/ml per counts/pixel. The y-intercept of -0.63 ± 0.93 kbeads/ml did not differ from zero in the limits of standard deviation.

The similar analysis was performed for all slices of four pigs. The κ-values in Table 1 varied for different hearts. According to Eq. (1a), the κ-value depends on both tissue optical properties and optical parameters of FM, excitation and emission collection (see Section 4.2.). Therefore, both factors may affect it. At present, it is impossible to distinguish them. However, once formally averaging, the resulting mean κ-value over all slices for all hearts was close to the value for the representative heart (Figure 5) with standard deviation from heart to heart (0.30 kbeads/ml per count/pixel) higher than for individual hearts (0.17–0.24 kbeads/ml per count/pixel; Table 1). Intercept was zero in the limits of standard deviation, and the correlation coefficient was also high. The high correlation coefficient and zero intercept obviously validate Eq. (1) for real cardiac tissue with non-uniform distribution of FM in the tissue.

3.3. Heart slices

The slope κ can be used as a factor in Eq. (1) to transfer the fluorescence image intensity to FM concentration at every pixel when the whole slice is under consideration. In the present study it was determined as described in Section 3.1. To obtain $(F_a + F_b)/2$ and apply Eq. (1) the slice was tightened between two glass plates in a special holder. A flip of the holder provides imaging of both sides (Figure 6A and 6B). The physical inversion of the slice was compensated by mathematical inversion of the matrix representing the image $I_{bi}(i, j) = I_b(n - i, j)$, where I_{bi} is the inverted image (Figure 6C) of the initial image I_b, i

and j are coordinates of a pixel, and n is the total number of pixels in the i-direction. Then the initial A-side image and inverted B-side images were superimposed $(I_a + I_{bi})/2$ resulting in the image corresponding to $(F_a + F_b)/2$ (Figure 6D). Finally, the image I_c of the FM content (Figure 6E) in the slice was obtained as:

$$I_c = \kappa \frac{I_a + I_{bi}}{2} \tag{2}$$

where κ was determined according to the procedure described in a Section 3.1. The final image can be used to choose regions of interest (ROI). The selection of ROIs has no restrains and provides an opportunity to calculate the FM content anywhere across the slice according to a research task.

Figure 6F shows an example of four ROIs for a representative slice. Results in Table 2 consist of the number of pixels in each ROI, the ROI physical area, the FM concentration in the ROI, their total number and heterogeneity of their distribution across the ROI estimated as a ratio of standard deviation to the mean value in percents as in Ref. [12]. The heterogeneity took place because of both variability of the blood vessel network inside the ROI and appearing the bright spots on a grey background (see below for discussion). Total number of FM in each ROI in respect of the FM content in whole slice (percentage) can serve as a measure at the estimation of variation of the blood flow through the heart.

The parameters indicated in Table 2 are specific for the slice. They vary because of the experimental choice of ROI size, shape and position, as well as physiological variability of the blood vessel network pattern in different slices across the heart [42, 43]. Therefore, a statistical analysis of the average values is impossible. To confirm a feasibility and repeatability of the approach, the results for nine different slices from two hearts were compiled and presented in an examples PDF file available online.
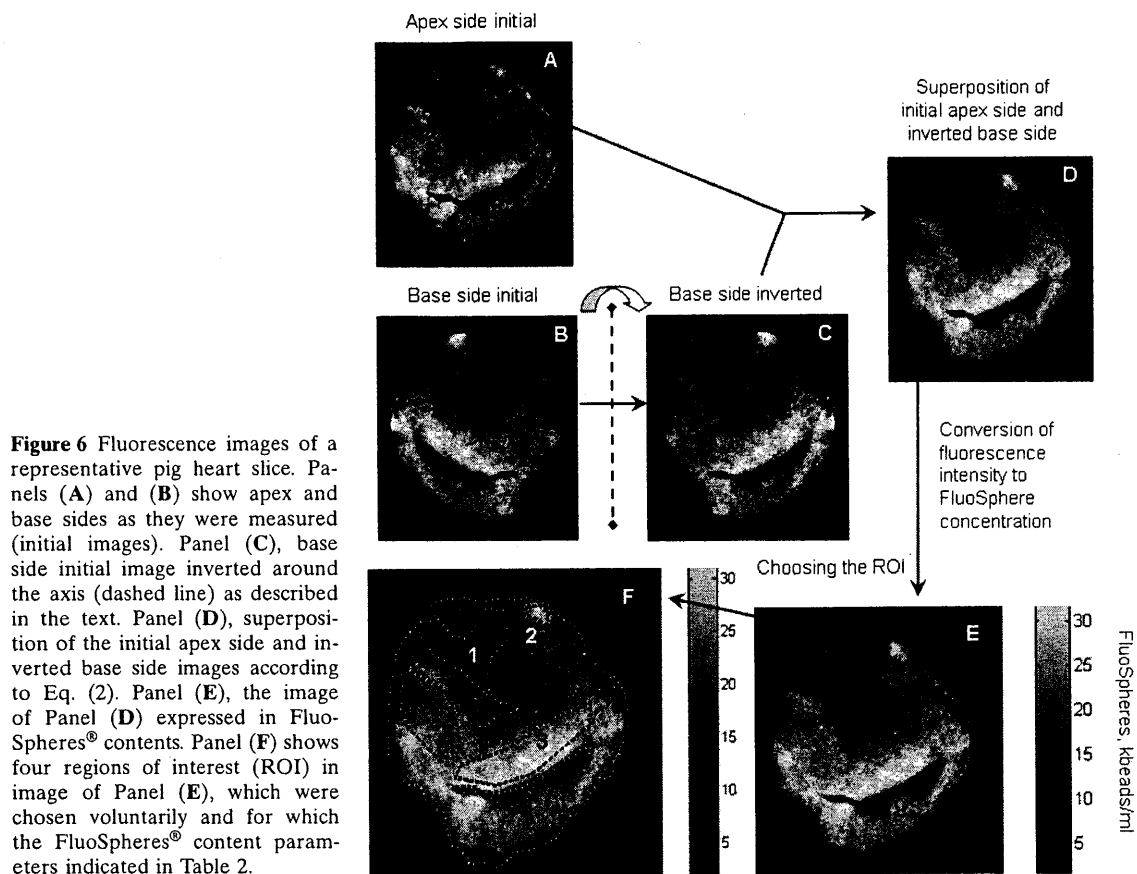
Apex side initial

Superposition of
initial apex side and
inverted base side

Base side initial   Base side inverted

Conversion of
fluorescence
intensity to
FluoSphere
concentration

Choosing the ROI

Figure 6 Fluorescence images of a representative pig heart slice. Panels (**A**) and (**B**) show apex and base sides as they were measured (initial images). Panel (**C**), base side initial image inverted around the axis (dashed line) as described in the text. Panel (**D**), superposition of the initial apex side and inverted base side images according to Eq. (2). Panel (**E**), the image of Panel (**D**) expressed in FluoSpheres® contents. Panel (**F**) shows four regions of interest (ROI) in image of Panel (**E**), which were chosen voluntarily and for which the FluoSpheres® content parameters indicated in Table 2.

Table 2 FluoSpheres® (FM) in the pig heart slice deduced from fluorescence imaging data by Eq. (2).

ROI	Number of pixels	Area, cm^2	FM content, $kbeads/cm^3$	Heterogeneity, %	Total FM, kbeads	Total FM, %
1	3027	2.42	10.5 ± 1.7	16.7	18.3	4.2
2	240	0.19	27.2 ± 3.8	13.9	3.8	0.9
3	3317	2.65	30.1 ± 4.1	13.5	57.5	13.3
4	2777	2.22	22.1 ± 3.3	16.0	35.4	8.2
Whole slice	37334	29.87	20.2 ± 7.2	35.8	433.4	100

Notes. FM, fluorescent microspheres; ROI, region of interest (see Figure 6F). Area was calculated using the conversion factor of $0.283^2 = 0.080$ mm²/pixel (see text). "±" in FM content means a standard deviation (SD) of the bead content over the ROI. Heterogeneity was calculated as SD per FM content in percents. Number of pixels and area data for whole slice relate to the tissue only and do not include the holes as shown in Figure 6F.

3.4. Spatial resolution

The same fluorescence image of a representative slice was captured at two different spatial resolutions of 197 and 37.4 μm per linear pixel size (0.039 and 0.0014 mm² per pixel, respectively; Figure 7). The resolution variation was done by changing the distance between slice plane and CCD camera lens. Both Figures 6 and 7 show that the fluorescence image of a cardiac slice consisted of bright spots on a grey background. No fluorescence (black background) related to non-tissue areas on the image. Bright spots on the higher resolution image (Figure 7B) have diameter of about 100–140 μm.
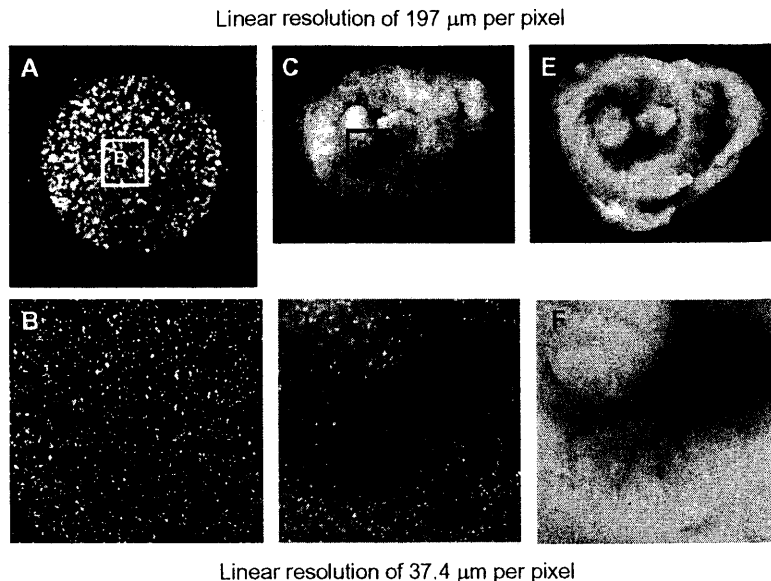
Linear resolution of 197 μm per pixel

Figure 7 (A) representative pig heart slice fluorescence image at resolutions of 197 μm pixel size in panel (C) and 37.4 μm pixel size in panel (D). Panel (D) image is a part of image in panel (C) as shown. The same slice at the same two resolutions at white illumination (no fluorescence) is shown in Panels (E) and (F), respectively. Fluorescence images of Fluo-Spheres® adsorbed in Millipore 5 μm filter from water suspension of 8 kbeads/ml are shown in Panels (A) and (B) for two resolutions. Panel (B) is a part of the Panel (A) image as shown. Variation of the resolution resulted from variation of the distance between lens and sample (see Figure 2).

Linear resolution of 37.4 μm per pixel

It was impossible to resolve the bright points with the optical capability of the image capture system (see Material and Methods). However, even at the higher optical resolution, the fine structure of the fluorescent points may not be resolved owing to the diffuse nature of both the excitation light penetration into the tissue and fluorescence emitted from the slice surface and underlying tissue layers. Obviously, the grey background on the slice images resulted from such diffusion of fluorescence emitted from FM inside the tissue, because no grey background was found on the image of FM adsorbed only on the surface of Millipore filter. There was no FM in the filter depth (Figures 7A and B).

Therefore, the fluorescent point sizes of 100–140 μm may result from both overlapping images from layers of increasing depth and the diffuse nature of light propagation in the heart tissue. Accordingly, the improved optical resolution may be ineffective for this purpose.

4. Discussion

4.1. Advantages of the fluorescence imaging approach

4.1.1 Non-destructiveness

Any "digestion & extraction" approach implies the cutting of the sample, which is an invasive and blind-type procedure when it is *a priori* unknown where

the FM are located. After the sample to be analyzed is cut and the FM contents in the cuts are found, it is impossible to change the scheme of the cut sampling. Quantitative fluorescence tissue imaging is a non-invasive procedure. Once the image is captured, it allows redefining the areas of interest and recalculation of the FM content. Such redefinition can be repeated as many times as needed with any number of ROIs not exceeding the number of pixels.

4.1.2. High spatial resolution

Spatial resolution for the "digestion & extraction" method is quite low. It is easy to estimate that for a 5 mm thick slice of 1.06 g/ml density (muscle), cut into pieces of about 0.1 g, the area is 0.19 cm² or 4.3 × 4.3 mm. Fluorescence imaging provides resolution of a few orders of magnitude higher approaching 50–100 μm (linear) or 0.002–0.01 mm² (area). This resolution could be close to a single FM particle size. However, the diffuse nature of light propagation in the muscle tissue decreases the fluorescence imaging resolution and doesn't allow a single particle size determination. The high spatial resolution allows determination of the sample heterogeneity in terms of FM distribution, which may be linked to heterogeneity of blood microcirculation in the tissue.

Obviously, a spatial resolution of the FM concentration images is limited not only by the spatial resolution of the fluorescence image capture. A reduction of this resolution may arise from uncertainty appeared at the mechanical flip of the slice. In our

case, a linear accuracy of the flip was about half a millimeter. Comparison of Figure 6A and E shows that the bright spots on the FM concentration image are smoother than in the fluorescence image. It may be because of both the mechanical flip problem and difference in the blood vessel distribution between apex and base sides of the slice.

4.1.3. Low time consuming

The "digestion & extraction" approach requires time for the sample digestion, the FM particles separation, dissolving them in organic solvent to release the dye, and finally the fluorescent dye concentration determination. This procedure requires many hours or even days [44]. Automation of the procedure may reduce the time consumed for the analysis of large number of samples but it is still in the hours range. Fluorescence imaging itself requires a couple of seconds for measurement. When the sample is a slice, it requires a minute to insert the sample into a chamber and take it out. The image file downloading and a Matlab program operation takes an additional minute. In total, the time needed is a couple of minutes.

4.1.4. Simplicity

No chemicals are needed for the fluorescence imaging in contrast to the "digestion & extraction". No radioactive materials, films, and related precautions are required in contrast to the RM method, while the radioactive and fluorescent microsphere measurements of myocardial blood flow were found equivalent [44–46].

4.1.5. Repeatability of analysis

There are two levels of repeatability. Firstly, any piece of tissue can be fluorescently imaged as many times as necessary because of the non-invasive character of the analysis. When the tissue piece is kept in a preservative like buffered formalin, the imaging can be performed in a long time after the tissue harvesting. Low concentration of formaldehyde in the buffered formalin does not allow significantly affect FM buried in blood vessels. From our experience, pig heart slices kept in buffered formalin for a month or more did not show a degradation of the fluorescence pattern.

Secondly, in each image, the ROI can be chosen as many times as necessary.

4.2. Miscellaneous

The slope is a coefficient κ in Eq. (1) or (2) and hence depends (i) on the tissue structure which determines the reduced scattering coefficient μ'_s, (ii) on the extinction coefficient ε and fluorescence quantum yield φ of the FM dye, and (iii) on an experimental setup including lens aperture, excitation light intensity E_0, camera sensitivity, integration time of the signal capture, gain etc.. Therefore, the slope is not a universal coefficient and must be determined each time when tissue, FM, excitation light and other parameters of the experimental setup are modified.

References

[1] R. W. Glenny, S. Bernard, and M. Brinkley, J. Appl. Physiol. **74**, 2585–2597 (1993).

[2] M. F. M. van Oosterhout, H. M. M. Willifgers, R. S. Reneman, and F. W. Prinzen, Am. J. Physiol Heart Circ. Physiol. **269**, H725–H738 (1995).

[3] M. F. M. van Oosterhout, F. W. Prinzen, S. Sakurada, R. W. Glenny, and J. R. Hales, Am. J. Physiol. Heart Circ. Physiol. **275**, H110–H115 (1998).

[4] D. Deveci and S. Egginton, Exper. Physiol. **84**, 615–630 (1999).

[5] S. L. Bernard, J. R. Ewen, C. H. Barlow, J. J. Kelly, S. McKinney, D. A. Frazer, and B. W. Glenny, Am. J. Physiol. Heart Circ. Physiol. **279**, H2043–H2052 (2000).

[6] Y. K. M. Decking, V. M. Pai, E. Bennett, J. L. Taylor, C. D. Fingas, K. Zanger, H. Wen, and R. S. Balaban, Am. J. Physiol. Heart Circ. Physiol. **287**, H1132–H1140 (2004).

[7] S. Raab, E. Thein, A. G. Harris, and K. Messmer, Am. J. Physiol. Heart Circ. Physiol. **276**, H1801–H1806 (1999).

[8] E. Thein, S. Raab, A. G. Harris, and K. Messmer Comput. Meth. Progr. Biomed. **61**, 11–21 (2000).

[9] F. W. Prinzen and R. W. Glenny, Cardiovasc. Res. **28**, 1467–1475 (1994).

[10] S. Hale, M. T. Vivaldi, and R. A. Kloner, Am. J. Physiol. Heart Circ. Physiol. **251**, H863–H868 (1986).

[11] L. W. V. DeBoer, H. W. Strauss, R. A. Kloner, R. E. Rude, R. F. Davis, P. R. Maroko, and E. Braunwald, P. Natl. Acad. Sci. USA **77**, 6119–6123 (1980).

[12] T. Matsumoto, H. Tachibana, Y. Ogasawara, and F. Kajiya, Am. J. Physiol. Heart Circ. Physiol. **280**, H465–H474 (2001).

[13] B. Khoobehi, B. Shoelson, Y. Z. Zhang, and G. A. Peyman, Ophtal. Surg. Laser **28**, 937–947 (1997).

[14] V. Chernomordik, D. Hattery, I. Gannot, and A. H. Gandjbakhche, IEEE J. Sel. Top. Quant. Electron. **5**, 930–935 (1999).

[15] J. Chang, H. L. Graber, and R. L. Barbour, IEEE Trans. Biomed. Eng. **44**, 810–822 (1997).

[16] D. Y. Paithankar, A. U. Chen, B. W. Pogue, M. S. Patterson, and E. M. Sevick-Muraca, Appl. Optics **36**, 2260–2272 (1997).

[17] E. Gussakovsky and Y. Yang, J. Fluoresc. (2010). DOI: 10.1007/s10895–010-0629-x.

[18] V. V. Turchin, Tissue optics: Light scattering methods and instrumentation for medical diagnostics (SPIE Press, Bellingham, 2007).

[19] J. F. Beek, H. J. van Staveren, P. Posthumus, H. J. C. M. Sterenberg, and M. J. C. van Gemert, In: G. Müller, B. Chance, R. R. Alfano, S. R. Arridge, J. Beuthan, E. Gratton, M. Kaschke, B. R. Masters, S. Svanberg, and P. van der Zee (eds.) Medical Optical Tomography: Functional Imaging and Monitoring (SPIE Press, Bellingham, Wash., 1993), vol. IS11, pp. 193–210.

[20] A. E. Arai, C. E. Kasserra, P. R. Territo, A. H. Gandjbakhche, and R. S. Balaban, Am. J. Physiol. Heart Circ. Physiol. **277**, H683–H697 (1999).

[21] W. G. Zijlstra, A. Buursma, and O. W. van Assendelft, Visible and near infrared absorption spectra of human and animal haemoglobin. Determination and application (VSP BV, Utrecht, 2000).

[22] E. Gussakovsky, O. Jilkina, Y. Yang, and V. Kupriyanov, Anal. Biochem. **383**, 107–115 (2008).

[23] E. Gussakovsky and V. Kupriyanov, Appl. Spectrosc. **62**, 671–676 (2008).

[24] E. Gussakovsky, Proc. SPIE **7187**, 71871D/1–71871D/8 (2009).

[25] S. L. Meyer, Data analysis for scientists and engineers (John Wiley, New York, 1975).

[26] A. J. Durkin, S. Jaikumar, and R. Richards-Kortum, Appl. Spectrosc. **47**, 2114–2121 (1993).

[27] G. M. Palmer, C. Zhu, T. M. Breslin, F. Xu, K. W. Gilchrist, and N. Ramanujam, Appl. Optics **45**, 1072–1078 (2006).

[28] Y. S. Fawzy and H. Zeng, Appl. Optics **45**, 3902–3912 (2006).

[29] G. Zonios, L. T. Perelman, V. Backman, R. Manohatran, M. Fitzmaurice, J. Van Dam, and M. S. Feld, Appl. Optics **38**, 6628–6637 (2002).

[30] M. Mirenda, M. G. Lagorio, and E. San Roman, Langmuir **20**, 3690–3697 (2004).

[31] F. Fabbri, M. A. Franceschini, and S. Fantini, Appl. Optics **42**, 3063–3072 (2003).

[32] J. C. Finlay and T. H. Foster, Optics Lett. **29**, 965–967 (2004).

[33] S. C. Gebhart, A. Mahadevan-Jansen, and W.-C. Lin, Appl. Optics **44**, 4884–4901 (2005).

[34] N. M. Marin, A. Milbourne, H. Rhodes, T. Ehlen, D. Miller, L. Benedet, R. Richards-Kortum, and M. Follen, Gynecol. Oncol. **99**, S116–S120 (2005).

[35] H. J. van Staveren, C. J. M. Moes, J. van Marle, S. A. Prahl, and M. J. C. van Gemert, Appl. Optics **30**, 4507–4514 (1991).

[36] S. T. Flock, S. L. Jacques, B. C. Wilson, W. M. Star, and M. J. C. van Gemert, Laser Surg. Med. **12**, 510–519 (1992).

[37] G. Wagnieres, S. Cheng, M. Zellweger, N. Utke, D. Barichotte, J.-P. Ballini, and H. van den Bergh, Phys. Med. Biol. **42**, 1415–1426 (1997).

[38] J. Swartling, J. S. Dam, and S. Anderson-Engels, Appl. Optics **42**, 4612–4620 (2003).

[39] K. Sokolov, J. Galvan, A. Myakov, A. Lacy, R. Lotan, and R. Richards-Kortum, J. Biomed. Optics **7**, 148–156 (2002).

[40] A. Springsteen, Anal. Chim. Acta **380**, 379–390 (1999).

[41] J. Mendez and A. Key, Metabolism **9**, 184–188 (1960).

[42] K. K. Griendling, and R. W. Alexander, in: R. C. Schlant and D. W. Alexander (eds.) The heart arteries and veins (McGraw-Hill, New York, 1994), pp. 21–46.

[43] S. M. Factor and R. J. Bache, in: R. C. Schlant and D. W. Alexander (eds.) The heart arteries and veins (McGraw-Hill, New York, 1994), pp. 1033–1054.

[44] W. Tan, K. W. Riggs, R. L. Thies, and D. W. Rurak, Can. J. Physiol. Pharmacol. **75**, 959–968 (1997).

[45] G. L. Chien, C. G. Anselone, R. F. Davis, and D. M. van Winkle, Cardiovasc. Res. **30**, 405–412 (1995).

[46] E. Thein, S. Raab, A. G. Harris, M. Kleen, O. Habler, F. Meisner, and K. Messmer, Eur. Surg. Res. **34**, 215–223 (2002).